Rapid Communications

High-order moments of streamwise fluctuations in a turbulent channel flow with spanwise rotation

Zhenhua Xia*
Department of Engineering Mechanics and Key Laboratory of Soft Machines and Smart Devices of Zhejiang Province, Zhejiang University, Hangzhou 310027, China

Geert Brethouwer
Linné FLOW Centre and Swedish e-Science Research Centre, KTH Mechanics, SE-100 44 Stockholm, Sweden

Shiyi Chen
Department of Mechanics and Aerospace Engineering, Southern University of Science and Technology, Shenzhen 518055, China;
State Key Laboratory for Turbulence and Complex Systems, Peking University, Beijing 100871, China; and Department of Engineering Mechanics, Zhejiang University, Hangzhou 310027, China

(Received 13 December 2017; published 13 February 2018)

It is well known that the spanwise rotation in turbulent channel flow alters the mean velocity distribution to a linear law. In the present work, we have studied the higher-order moments of the streamwise fluctuations in a turbulent channel flow with spanwise rotation. Our results show that in a significant part of the channel the $2p$-order moments, raised by the power $1/p$ with $p = 1,2,\ldots,6$, also follow linear behavior according to $\langle (u'^{+})^{2p}\rangle^{1/p} = a_p(y/h) + b_p$. Here, u'^{+} is the streamwise velocity fluctuation normalized by the global friction velocity, h is the channel half width, and b_p and a_p are the intercept and the slope, respectively, which vary with Reynolds and rotation numbers. The linear regions can be extended by introducing a self-similar scaling, that is, $2p$-order moments as a function of $2q$-order moments. The slopes in the self-similar scaling a_p/a_1 do not reveal sub-Gaussian behavior as in nonrotating wall-bounded flows, but rather Gaussian or super-Gaussian behaviors.

DOI: 10.1103/PhysRevFluids.3.022601

Wall-bounded turbulence is ubiquitous in nature as well as engineering applications, and it has been studied extensively. In wall-bounded turbulence without separations or system rotation, the most well-known feature is the universal logarithmic relation between the mean streamwise velocity and the distance to the wall (y) in the inertial region [1–3], that is,

$$\langle u\rangle/u_\tau \equiv \langle u\rangle^{+} = \frac{1}{\kappa}\ln\left(\frac{u_\tau y}{\nu}\right) + C.$$

Here, $u_\tau = \sqrt{\tau_w/\rho}$ is the friction velocity based on the wall friction stress τ_w and the fluid density ρ, ν is the kinematic viscosity, κ is the von Kármán constant, and C is the intercept of the logarithmic law, which is also a constant at high Reynolds number. Many experimental and numerical studies of turbulent boundary layer, turbulent pipe flow, and turbulent channel flows have shown evidence of the above logarithmic law (see the reviews [4–6], and references therein).

*Author to whom correspondence should be addressed: xiazh@zju.edu.cn

In addition to the mean streamwise velocity, the velocity fluctuations are very important quantities for wall-bounded turbulence, and another logarithmic behavior, motivated by the "attached eddy hypothesis" [7–9], was reported for the variance of the streamwise velocity fluctuations in the inertial region [5,10–14],

$$\left\langle (u'^{+})^2 \right\rangle = B_1 - A_1 \ln(y/\delta).$$

Here, $u'^{+} = (u - \langle u \rangle)/u_\tau$ is the normalized streamwise velocity fluctuation, δ is the outer length scale, which is half of the channel width for a channel flow, the radius for a pipe flow, or the boundary layer thickness for a boundary layer flow. $A_1 \approx 1.25$ is the Townsend-Perry constant [5,10,12–15] while B_1 is a parameter which depends on flow conditions and geometry. More recently, Meneveau and Marusic [16] found that the pth root of the $2p$-order moments of the streamwise velocity fluctuations also follow a generalized logarithmic law,

$$\langle (u'^{+})^{2p} \rangle^{1/p} = B_p - A_p \ln(y/\delta) = D_p(\mathrm{Re}_\tau) - A_p \ln(y^{+}), \tag{1}$$

where $y^{+} = y/l_\nu = y u_\tau/\nu$ is the wall distance in viscous units, $\mathrm{Re}_\tau = u_\tau \delta/\nu$ is the friction Reynolds number, $D_p = B_p + A_p \ln \mathrm{Re}_\tau$ is a Reynolds-number-dependent offset, and A_p is the slope of the logarithmic law. They reported that the slopes A_p, which are lower than the Gaussian prediction $A_1[(2p-1)!!]^{1/p}$, appear quite insensitive to the Reynolds number, suggesting the existence of universal behavior in wall-bounded turbulence. This generalized logarithmic law for high-order moments can also be explained by the attached eddy hypothesis, assuming that the eddy population density is inversely proportional to the wall distance while the length scales of the eddies are directly proportional to the wall distance [16–18]. Furthermore, by using this attached eddy hypothesis, other logarithmic scalings of generalized high-order two-point correlations can be motivated. These were confirmed for turbulent boundary layer [18,19]. These logarithmic scalings can also be predicted using momentum generating functions [20,21] and have been observed in large-eddy simulation [22]. Generalized high-order statistics can be used as a diagnostic tool in numerical simulations as well as experimental measurements [23,24].

Wall-bounded turbulence with system rotation is of great interest to engineering applications, geophysics, as well as astrophysics. As one typical well-defined canonical flow problem, turbulent channel flow subject to spanwise rotation has attracted a lot of attention from theoretical, experimental and numerical points of view [25–46]. It is generally accepted for a spanwise-rotating turbulent channel flow (RTCF) that turbulence is augmented in the part of the channel where the mean flow vorticity has an opposite sign to the system rotation (anticyclonic rotation), while it is suppressed in the other part where the two quantities are of the same sign (cyclonic rotation). Spanwise rotation alters the flow structures and flow statistics strongly in turbulent channel flow, and the most famous result concerns the mean velocity profile. In RTCF, the mean velocity exhibits a linear profile with a slope $dU/dy \approx 2\Omega$ (here, U is the mean streamwise velocity and Ω is the spanwise angular velocity), which implies a nearly zero absolute mean vorticity. This linear mean velocity profile was first reported in the experimental results by Johnston *et al.* [25], and then verified by others by experiments and numerical simulations. Recently, Xia *et al.* [42] reported other linear profiles in RTCF by using their direct numerical simulation (DNS) results at low friction Reynolds number $\mathrm{Re}_\tau = 180$ ($\mathrm{Re}_\tau = u_\tau \delta/\nu$ with u_τ being the global friction velocity and ν being the kinematic viscosity), such as the Reynolds shear stress and the production of turbulent kinetic energy. The newly reported linear profiles were verified by Brethouwer [46] in DNS at higher Reynolds numbers.

Although RTCF has been intensively studied, very few results are reported on high-order statistics. In this Rapid Communication, the high-order moments of streamwise fluctuations will be studied using DNS data from Xia *et al.* [42] and Brethouwer [46]. It is interesting to see that these high-order moments also follow linear behaviors in a certain part of the channel although the Reynolds number is quite low. The dependence of the slopes on rotation and Reynolds numbers will also be discussed.

The present work is based on an analysis of the DNS data presented in Refs. [42,46]. Figure 1 shows the profiles of $\langle (u'^{+})^2 \rangle$ for different cases. In the DNS of Ref. [42] Re_τ was kept constant and the bulk Reynolds number $\mathrm{Re}_b = U_b \delta/\nu$, where U_b is the bulk mean velocity, varies with the

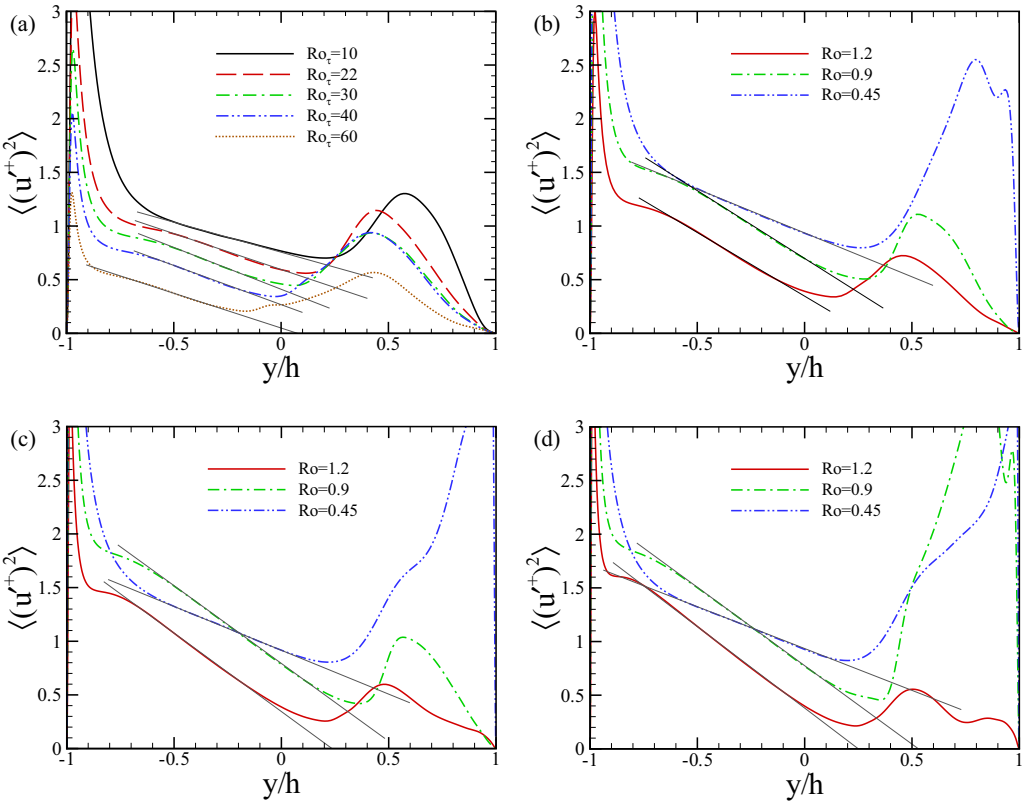

FIG. 1. Profiles of $\langle(u'^+)^2\rangle$. (a) results at $Re_\tau = 180$; (b) results at $\mathrm{Re}_b = 10\,000$; (c) results at $\mathrm{Re}_b = 20\,000$, and (d) results at $\mathrm{Re}_b = 31\,600$. The data are from Ref. [42] (a) and Ref. [46] (b)–(d). The thin solid lines show linear profiles with different slopes.

rotation rate, whereas in the DNS of [46] it was the other way around. When we refer to data from the first source we mention therefore Re_τ, whereas when we refer to data from the second source we mention Re_b. Tables with Re_τ together with Re_b, $\mathrm{Ro}_\tau = 2\Omega\delta/u_\tau$ and $Ro = 2\Omega\delta/U_b$ are given in both Refs. [42,46]. At lower Reynolds number cases as shown in Fig. 1(a), where the global friction Reynolds number is fixed at $\mathrm{Re}_\tau = 180$, $\langle(u'^+)^2\rangle$ decays with increasing rotation number Ro_τ on the unstable pressure side. Away from the wall on the pressure side, a linear relation

$$\langle(u'^+)^2\rangle = a_1(y/h) + b_1 \tag{2}$$

can be identified for all five Ro_τ. This is within the region where the mean velocity profile displays a linear slope. However, the slopes at different Ro_τ are not the same, but vary slightly. At higher Reynolds numbers, as displayed in Figs. 1(b)–1(d), where the bulk Reynolds numbers are fixed at $\mathrm{Re}_b = 10\,000$, 20 000, and 31 600, respectively, $\langle(u'^+)^2\rangle$ also has a linear slope away from the wall on the pressure side for all cases. The slopes vary more apparently than at lower Reynolds numbers. The linear slopes a_1 of $\langle(u'^+)^2\rangle$ are plotted as function of Ro and Ro_τ in Fig. 2. It is seen that a_1 first decreases with Ro or Ro_τ and then increases with Ro or Ro_τ at all Reynolds numbers considered. At lower Reynolds numbers, a_1 is above -1 and varies slowly with Ro. At higher Reynolds numbers, a_1 varies considerably with Ro, from a value around -0.8 at $\mathrm{Ro} = 0.45$ to a value around -1.5 at $\mathrm{Ro} = 0.9$ and 1.2 for $\mathrm{Re}_b \geqslant 20\,000$. Note that in the DNS of Ref. [46] with a constant Re_b, $\mathrm{Re}_\tau \leqslant 180$ for $\mathrm{Re}_b = 5000$ and $\mathrm{Ro} \geqslant 1.2$, whereas in all other DNS from that source $\mathrm{Re}_\tau > 180$. From the figure, we can infer that the slope varies more strongly with Ro at higher Reynolds numbers.

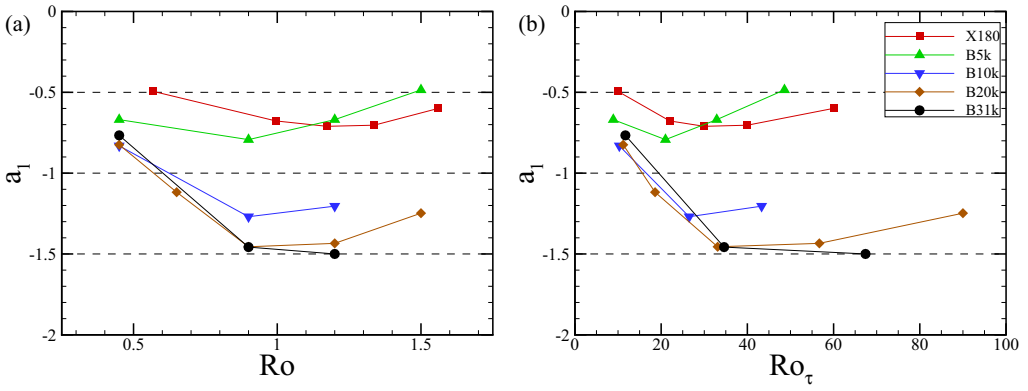

FIG. 2. Slopes a_1 for the linear fitting of $\langle(u'^+)^2\rangle$ as a function of (a) Ro and (b) Ro_τ. "X180" refers to the data from Ref. [42] at $\mathrm{Re}_\tau = 180$, while "B5k," "B10k," "B20k," and "B31k" refer to the data from Ref. [46] at $\mathrm{Re}_b = 5000,\ 10\,000,\ 20\,000$, and 31 600, respectively.

In nonrotating wall-bounded turbulence, the higher-order moments follow the same logarithmic behavior as the variance of the streamwise fluctuations $\langle(u'^+)^2\rangle$. In the present work, we have demonstrated that $\langle(u'^+)^2\rangle$ follows a linear law at different Reynolds and rotation numbers. Now, we are going to show that the higher-order moments also follow a linear behavior. Figures 3(a) and 4(a) show the profiles of $\langle(u'^+)^{2p}\rangle^{1/p}$ for $p = 1, \ldots, 6$ at $\mathrm{Re}_\tau = 180$, $\mathrm{Ro}_\tau = 22$, and $\mathrm{Re}_b = 31\,600$, $\mathrm{Ro} = 1.2$, respectively, the latter case corresponding to $\mathrm{Re}_\tau = 562$ and $\mathrm{Ro}_\tau = 67$. The linear fitting

$$\langle(u'^+)^{2p}\rangle^{1/p} = a_p(y/h) + b_p \tag{3}$$

is also shown in the figure. The corresponding fitting coefficients a_p and b_p and the adjusted R square for $p = 1, \ldots, 6$ are listed in Tables I and II, respectively. It is clearly seen that linear profiles can be discerned for $\langle(u'^+)^{2p}\rangle^{1/p}$ with $p = 1, \ldots, 6$ on the pressure side, again in the region where the mean velocity profile displays a linear slope. The higher-order moments of the two other velocity components (not shown) do not display a linear slope. In order to show more clearly how well is this linear fitting, the relative error of the linear fittings, which is defined as

$$\varepsilon = (\langle(u'^+)^{2p}\rangle^{1/p} - [a_p(y/h) + b_p])/\langle(u'^+)^{2p}\rangle^{1/p} = 1 - [a_p(y/h) + b_p]/\langle(u'^+)^{2p}\rangle^{1/p}, \tag{4}$$

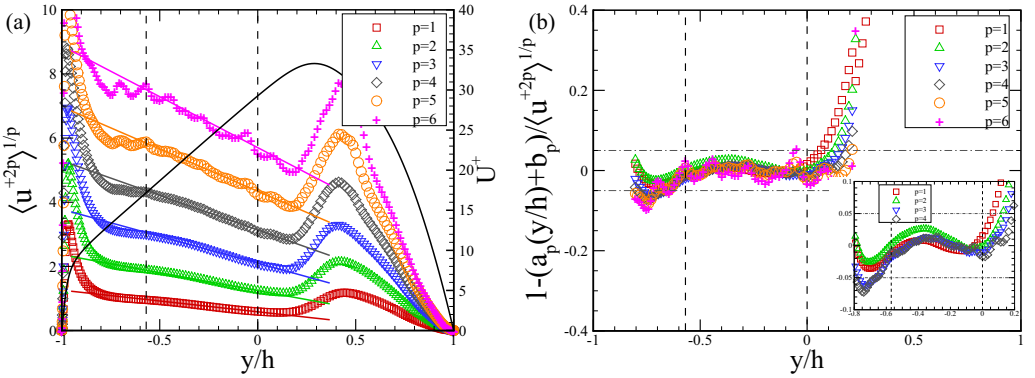

FIG. 3. (a) Profiles of $\langle(u'^+)^{2p}\rangle^{1/p}$ and their linear fittings $\langle(u'^+)^{2p}\rangle^{1/p} = a_p(y/h) + b_p$ for $p = 1$ to 6. U^+ is also plotted to show the linear region for mean velocity (black solid line). (b) Relative error of the linear fitting $1 - [a_p(y/h) + b_p]/\langle(u'^+)^{2p}\rangle^{1/p}$ for $p = 1$ to 6. The data is from Ref. [42] at $\mathrm{Ro}_\tau = 22$ and fitting coefficients are listed in Table I. Inset in (b) shows the zoomed-in behavior for $p = 1$ to 4.

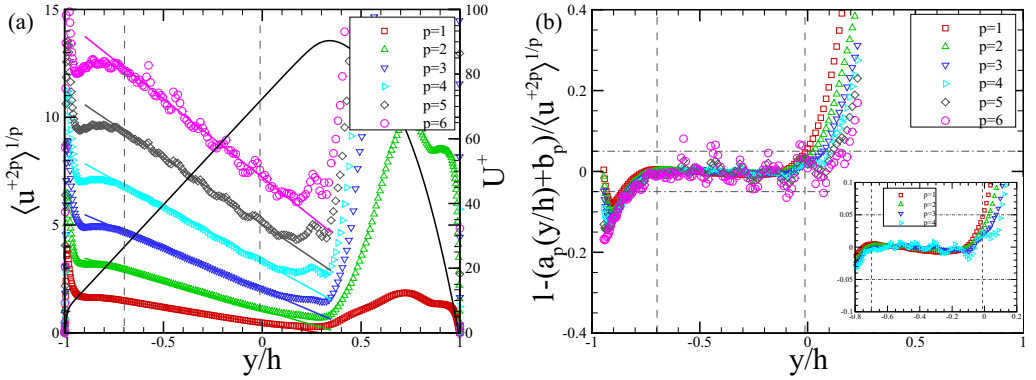

FIG. 4. (a) Profiles of $\langle (u'^{+})^{2p}\rangle^{1/p}$ and their linear fittings $\langle (u'^{+})^{2p}\rangle^{1/p} = a_p(y/h) + b_p$ for $p = 1$ to 6. U^+ is also plotted to show the linear region for mean velocity (black solid line). (b) Relative error of the linear fitting $1 - [a_p(y/h) + b_p]/\langle (u'^{+})^{2p}\rangle^{1/p}$ for $p = 1$ to 6. The data is from Ref. [46] at $\mathrm{Re}_b = 31\,600$ and $\mathrm{Ro} = 1.2$. Inset in (b) shows the zoomed-in behavior for $p = 1$ to 4.

is depicted in Figs. 3(b) and 4(b). It shows that the relative errors of these linear fittings are quite low; they are within 5% in the region $-0.7 \lesssim y/h \lesssim 0$ for most cases, which demonstrates the present good linear fittings. This is consistent with the adjusted R-square values listed in Tables I and II, which are larger than 0.94 for $p = 1$ to 6. It is seen in Figs. 3 and 4 that larger deviations exist for higher-order moments with $p \geqslant 5$; for lower-order moments with $p \leqslant 4$ the deviations are much smaller. In order to show the good fittings for lower-order moments, the relative errors for $p = 1, \ldots, 4$ are enlarged in the insets shown in Figs. 3(b) and 4(b). For the lower Reynolds number case, the relative errors are 3%, while in the higher Reynolds number case the errors are within 1% for $p \leqslant 4$. We may infer that the linear behavior is more apparent at high Reynolds numbers.

Figures 3(a) and 4(a) also include the mean velocity profiles U^+. This shows that the linear region for $\langle (u'^{+})^{2p}\rangle^{1/p}$ is smaller than the linear region for the mean velocity profile. This is in contrast to the nonrotating cases. In wall-bounded turbulence without system rotation, Marusic *et al.* [14] identified the logarithmic law for the mean velocity and $\langle (u'^{+})^{2}\rangle$ within the range $3\mathrm{Re}_\tau^{1/2} < y^+ < 0.15\,\mathrm{Re}_\tau$, while Meneveau and Marusic [16] found in the range $y^+ > 400$ and $y/\delta < 0.3$ (δ is the boundary layer thickness) a fit to the logarithmic laws for $\langle (u'^{+})^{2p}\rangle^{1/p}$. Stevens *et al.* [22], on the other hand, used the range $0.04 \leq y/\delta \leq 0.23$ to fit their large-eddy simulation data for $\langle (u'^{+})^{2p}\rangle^{1/p}$ to the logarithmic laws. In other words, in wall-bounded turbulence without system rotation, the logarithmic regions for the mean velocity and $\langle (u'^{+})^{2p}\rangle^{1/p}$ match and are within $y/\delta < 0.3$. In contrast, in spanwise-rotating turbulent channel flow, the linear profile for the mean velocity is quite wide (its extent is wider than $0.5h$ in some cases), while the linear regions for $\langle (u'^{+})^{2p}\rangle^{1/p}$ are much narrower. Furthermore, the extent of the region with these linear profiles depends on the Reynolds and rotation numbers.

In order to further verify the linear regions, plots of $\langle (u'^{+})^{2p}\rangle^{1/p}$ against $\langle (u'^{+})^{2}\rangle$ and $\langle (u'^{+})^{6}\rangle^{1/3}$ for $p = 1$ to 6 at $\mathrm{Re}_b = 31\,600$ and $\mathrm{Ro} = 1.2$ are depicted in Fig. 5. From Eq. (3), it is easy to obtain

TABLE I. Linear fitting information for the case with $\mathrm{Ro}_\tau = 22$ from Ref. [42]. The fitting region is $-0.5691 \leqslant y/h \leqslant 0$.

$y = a_p x + b_p$	$p = 1$	$p = 2$	$p = 3$	$p = 4$	$p = 5$	$p = 6$
a_p	−0.6736	−1.188	−1.682	−2.158	−2.637	−3.176
b_p	0.5843	1.244	2.099	3.135	4.342	5.703
Adjusted R square	0.9978	0.9954	0.9923	0.9921	0.9890	0.9417

TABLE II. Linear fitting information for the case with Ro = 1.2 and $\mathrm{Re}_b = 31\,600$ from Ref. [46]. The fitting region is $-0.6984 \leqslant y/h \leqslant -0.0123$.

$y = a_p x + b_p$	$p = 1$	$p = 2$	$p = 3$	$p = 4$	$p = 5$	$p = 6$
a_p	−1.500	−2.680	−3.889	−5.065	−6.174	−7.286
b_p	0.4405	1.054	1.985	3.296	5.035	7.206
Adjusted R square	0.9995	0.9998	0.9998	0.9991	0.9939	0.9616

a relation between $\langle (u'^+)^{2p} \rangle^{1/p}$ and $\langle (u'^+)^{2q} \rangle^{1/q}$,

$$\langle (u'^+)^{2p} \rangle^{1/p} = \frac{a_p}{a_q} \langle (u'^+)^{2q} \rangle^{1/q} + \frac{a_q b_p - a_p b_q}{a_q}, \tag{5}$$

where q is a positive integer that differs from p. This relation implies that a linear region can also be identified in the plot of $\langle (u'^+)^{2p} \rangle^{1/p}$ against $\langle (u'^+)^{2q} \rangle^{1/q}$ with the slope being a_p/a_q. A similar relation between high-order moments and mean velocity profiles was proposed by Örlü *et al.* [24] as a diagnostic scaling. It is apparent from Fig. 5 that linear regions can be obtained for $\langle (u'^+)^{2p} \rangle^{1/p}$ against $\langle (u'^+)^2 \rangle$ and $\langle (u'^+)^6 \rangle^{1/3}$ for $p = 1$ to 6 with slopes a_p/a_1 and a_p/a_3, respectively. More importantly, the linear regions with this new self-similar scaling are wider than the original ones with high-order moments profiles as a function of the wall distance, whose extent is marked by the two vertical dash-dotted lines in Fig. 5. Yang *et al.* [21] showed that the power-law scaling of the momentum generation functions (MGFs) for the streamwise velocity fluctuations can be extended to include the bulk and viscosity-affected regions $30 < y^+$, $y < \delta$ if the data were interpreted with a self-similar scaling of the MGFs as a function of one reference value, implying extended self-similarity [47–53]. Accordingly, our results also reveal extended self-similarity.

In fact, for wall-bounded turbulent flows without system rotation, we can also derive a self-similar scaling from Eq. (1)

$$\langle (u'^+)^{2p} \rangle^{1/p} = \frac{A_p}{A_q} \langle (u'^+)^{2q} \rangle^{1/q} + \frac{A_q B_p - A_p B_q}{A_q}, \tag{6}$$

which has the same form as Eq. (5). That is, the self-similar scaling of $\langle (u'^+)^{2p} \rangle^{1/p}$ as a function of $\langle (u'^+)^{2q} \rangle^{1/q}$ follows a linear law with the slope A_p/A_q in nonrotating wall-bounded turbulence, although $\langle (u'^+)^{2p} \rangle^{1/p}$ itself exhibits a logarithmic law. Specifically, if we set $q = 1$, then the slope

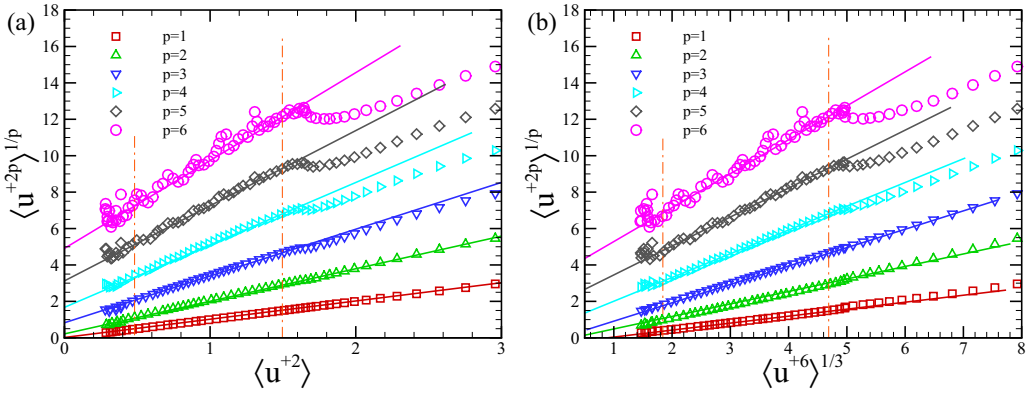

FIG. 5. (a) Plot of $\langle (u'^+)^{2p} \rangle^{1/p}$ against $\langle (u'^+)^2 \rangle$ for $p = 1$ to 6. The solid lines indicate the slopes a_p/a_1. (b) Plot of $\langle (u'^+)^{2p} \rangle^{1/p}$ against $\langle (u'^+)^6 \rangle^{1/3}$ for $p = 1$ to 6. The solid lines indicate the slopes a_p/a_3, while the vertical dash-dotted lines show the bounds of the linear regions depicted in Fig. 4 with $-0.6984 \leqslant y/h \leqslant -0.0123$. The data is from Ref. [46] at $\mathrm{Re}_b = 31\,600$ and Ro = 1.2.

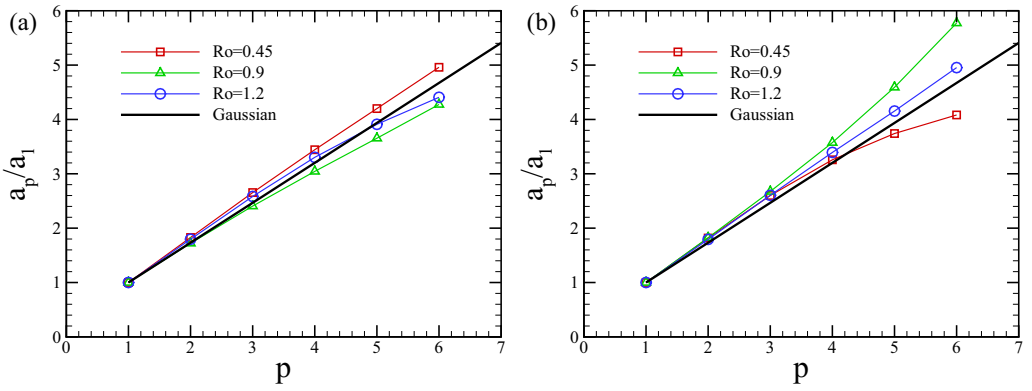

FIG. 6. Slopes of the self-scaling a_p/a_1 at different Reynolds number and rotation number. (a) $\mathrm{Re}_b = 20\,000$ and (b) $\mathrm{Re}_b = 31\,600$. The Gaussian values are also shown for comparison.

becomes A_p/A_1. As shown by Meneveau and Marusic [16], if the streamwise fluctuations have a Gaussian behavior, then $A_p/A_1 = [(2p-1)!!]^{1/p}$. However, in the wall-bounded turbulent flows without system rotation, the streamwise fluctuations display sub-Gaussian statistics and the slope A_p/A_1 falls below the Gaussian values $[(2p-1)!!]^{1/p}$. In spanwise-rotating turbulent channel flows, the system rotation complicates the flow statistics. In Fig. 6, the self-scaling slopes a_p/a_1 at $\mathrm{Re}_b = 20\,000$ and 31 600 are shown with reference to Gaussian values. Different from the nonrotating cases, the statistics are no longer sub-Gaussian for most cases considered, but approximately Gaussian or super-Gaussian. However, there is no clear agreement for the results at the two Re_b, implying that we cannot draw strong conclusions regarding the Gaussian or super-Gaussian behavior.

As presented above, the attached eddy hypothesis can be used to predict the logarithmic scaling of the single-point high-order moments of the streamwise velocity fluctuations in wall-bounded turbulent flows without system rotation. Brethouwer [46] found evidence that attached eddies also populate spanwise-rotating channel flow at lower rotation rates, but at higher rotation rates (e.g., $\mathrm{Ro} \gtrsim 0.9$ and $\mathrm{Re}_b = 20\,000$), they appear much less prominent. Therefore, we cannot use the attached eddy hypothesis to explain the linear profiles observed in spanwise-rotating channel flows. Nevertheless, if we adopted the attached eddy hypothesis but assumed that the eddy population density is constant in a certain region, it would lead to a linear profile for the even-order moments of the streamwise velocity fluctuations. However, a constant eddy population is very unlikely, therefore, this proposition is unlikely to give the correct physical explanation. As for the zero-absolute-mean-vorticity region of the mean velocity profile, more work needs to be done to find a proper physical explanation.

In conclusion, we studied the high-order moments of the streamwise fluctuations in spanwise-rotating turbulent channel flows. Our results showed that the high-order moments follow linear laws like the mean streamwise velocity. The linear regions for the higher-order moments are narrower than that for the mean velocity, but the linear regions can be extended if a self-similar scaling is used. Furthermore, our analysis showed that the flow statistics are no longer sub-Gaussian if the system rotates about the spanwise direction, but are approximately Gaussian or super-Gaussian. However, the Reynolds numbers studied are quite low. Data at higher Reynolds numbers should be used to further investigate the Reynolds and rotation number effect. Further studies are also required to find a proper physical explanation for the observed scaling behaviors.

Z.X. and S.C. acknowledge the financial support provided by National Natural Science Foundation of China (Grants No. 11772297 and No. 11521091). G.B. acknowledges PRACE for providing the computational resources at the Jülich Supercomputing Centre in Germany, and SNIC for providing the computational resources in Sweden. G.B. further acknowledges the support of the Swedish Research Council (Grant No. 621-2016-03533).

[1] L. Prandtl, Bericht uber untersuchungen zur ausgebildeten turbulenz, Z. Angew. Math. Mech. **5**, 136 (1925).
[2] T. von Kármán, Mechanische ähnlichkeit und turbulenz, in *Proceedings of the Third International Congress for Applied Mechanics* (Sveriges Litografiska Tryckerier, Stockholm, 1930), Vol. 1, pp. 79–93.
[3] S. B. Pope, *Turbulent Flows* (Cambridge University Press, Cambridge, UK, 2000).
[4] I. Marusic, B. J. McKeon, P. A. Monkewitz, A. J. Smits, and K. R. Sreenivasan, Wall-bounded turbulent flows at high Reynolds numbers: Recent advances and key issues, Phys. Fluid **22**, 065103 (2010).
[5] A. J. Smits, B. J. McKeon, and I. Marusic, High-Reynolds number wall turbulence, Annu. Rev. Fluid Mech. **43**, 353 (2011).
[6] J. Jiménez, Cascades in wall-bounded turbulence, Annu. Rev. Fluid Mech. **44**, 27 (2012).
[7] A. A. Townsend, *Structure of Turbulent Shear Flow* (Cambridge University Press, Cambridge, UK, 1976), Vol. 2.
[8] A. E. Perry and M. S. Chong, On the mechanism of wall turbulence, J. Fluid Mech. **119**, 173 (1982).
[9] A. E. Perry, S. M. Henbest, and M. S. Chong, A theoretical and experimental study of wall turbulence, J. Fluid Mech. **165**, 163 (1986).
[10] I. Marusic and G. J. Kunkel, Streamwise turbulence intensity formulation for flat-plate boundary layers, Phys. Fluids **15**, 2461 (2003).
[11] J. Jiménez and S. Hoyas, Turbulent fluctuations above the buffer layer of wall-bounded flows, J. Fluid Mech. **611**, 215 (2008).
[12] I. Marusic, The logarithmic region of wall turbulence: Universality, structure and interactions, in *Proceedings of the 18th Australasian Fluid Mechanics Conference, 2012*, edited by P. A. Brandner and B. W. Pearce (Australasian Fluid Mechanics Society, 2012).
[13] M. Hultmark, M. Vallikivi, S. C. C. Bailey, and A. J. Smits, Turbulent Pipe Flow at Extreme Reynolds Numbers, Phys. Rev. Lett. **108**, 094501 (2012).
[14] I. Marusic, J. P. Monty, M. Hultmark, and A. J. Smits, On the logarithmic region in wall turbulence, J. Fluid Mech. **716**, R3 (2013).
[15] M. Hultmark, A theory for the streamwise turbulent fluctuations in high Reynolds number pipe flow, J. Fluid Mech. **707**, 575 (2012).
[16] C. Meneveau and I. Marusic, Generalized logarithmic law for high-order moments in turbulent boundary layers, J. Fluid Mech. **719**, R1 (2013).
[17] J. D. Woodcock and I. Marusic, The statistical behaviour of attached eddies, Phys. Fluids **27**, 015104 (2015).
[18] X. I. A. Yang, I. Marusic, and C. Meneveau, Hierarchical random additive process and logarithmic scaling of generalized high order, two-point correlations in turbulent boundary layer flow, Phys. Rev. Fluids **1**, 024402 (2016).
[19] C. M. de Silva, I. Marusic, J. D. Woodcock, and C. Meneveau, Scaling of second- and higher-order structure functions in turbulent boundary layers, J. Fluid Mech. **769**, 654 (2015).
[20] X. I. A. Yang, I. Marusic, and C. Meneveau, Moment generating functions and scaling laws in the inertial layer of turbulent wall-bounded flows, J. Fluid Mech. **791**, R2 (2016).
[21] X. I. A. Yang, C. Meneveau, I. Marusic, and L. Biferale, Extended self-similarity in moment-generating-functions in wall-bounded turbulence at high Reynolds number, Phys. Rev. Fluids **1**, 044405 (2016).
[22] R. J. A. M. Stevens, M. Wilczek, and C. Meveveau, Large-eddy simulation study of the logarithmic law for second- and higher-order moments in turbulent wall-bounded flow, J. Fluid Mech. **757**, 888 (2014).
[23] D. I. Pullin, M. Inoue, and N. Saito, On the asymptotic state of high Reynolds number, smooth-wall turbulent flows, Phys. Fluids **25**, 015116 (2013).
[24] R. Örlü, A. Segalini, J. Klewicki, and P. H. Alfredsson, High-order generalisation of the diagnostic scaling for turbulent boundary layer, J. Turbul. **17**, 664 (2016).
[25] J. P. Johnston, R. M. Halleen, and D. K. Lezius, Effects of spanwise rotation on the structure of two-dimensional fully developed turbulent channel flow, J. Fluid Mech. **56**, 533 (1972).
[26] P. H. Alfredsson and H. Persson, Instabilities in channel flow with system rotation, J. Fluid Mech. **202**, 543 (1989).

[27] K.-S. Yang and J. Kim, Numerical investigation of instablility and transition in rotating plane Poiseuille flow, Phys. Fluids A **3**, 633 (1990).
[28] D. K. Tafti and S. P. Vanka, A numerical study of the effects of spanwise rotation on turbulent channel flow, Phys. Fluids A **3**, 642 (1990).
[29] R. Kristoffersen and H. I. Andersson, Direct simulations of low-Reynolds-number turbulent flow in a rotating channel, J. Fluid Mech. **256**, 163 (1993).
[30] K. Nakabayashi and O. Kitoh, Low Reynolds number fully developed two-dimensional turbulent channel flow with system rotation, J. Fluid Mech. **315**, 1 (1996).
[31] E. Lamballais, M. Lesieur, and O. Métais, Effects of spanwise rotation on the vorticity stretching in transitional and turbulent channel flow, Int. J. Heat Fluid Flow **17**, 324 (1996).
[32] K. Alvelius, Studies of turbulence and its modeling through large eddy- and direct numerical simulation, Ph.D. thesis, Department of Mechanics, KTH, Stockholm, Sweden, 1999.
[33] Y. Nagano and H. Hattori, Direct numerical simulation and modeling of spanwise rotating channel flow with heat transfer, J. Turbul. **4**, N10 (2003).
[34] Y. Maciel, D. Picard, G. Yan, and G. Dumas, Fully developed turbulent channel flow subject to system rotation, in *Proceedings of the 33rd AIAA Fluid Dynamics Conference and Exhibit, Orlando, Florida, 23-26 June 2003* (AIAA, Reston, VA, 2003), paper 2003-4153.
[35] K. Nakabayashi and O. Kitoh, Turbulence characteristics of two-dimensional channel flow with system rotation, J. Fluid Mech. **528**, 355 (2005).
[36] N.-S. Liu and X.-Y. Lu, Direct numerical simulation of spanwise rotating turbulent channel flow with heat transfer, Int. J. Numer. Methods Fluids **53**, 1689 (2007).
[37] O. Grundestam, S. Wallin, and A. V. Johansson, Direct numerical simulations of rotating turbulent channel flow, J. Fluid Mech. **598**, 177 (2008).
[38] Y. T. Yang and J. Z. Wu, Channel turbulence with spanwise rotation studied using helical wave decomposition, J. Fluid Mech. **692**, 137 (2012).
[39] D. P. Wall and M. Nagata, Three-dimensional exact coherent states in rotating channel flow, J. Fluid Mech. **727**, 533 (2013).
[40] S. Wallin, O. Grundestam, and A. V. Johansson, Laminarization mechanisms and extreme amplitude states in rapidly rotating plane channel flow, J. Fluid Mech. **730**, 193 (2013).
[41] G. Brethouwer, P. Schlatter, Y. Duguet, D. S. Henningson, and A. V. Johansson, Recurrent Bursts via Linear Processes in Turbulent Environments, Phys. Rev. Lett. **112**, 144502 (2014).
[42] Z. Xia, Y. Shi, and S. Chen, Direct numerical simulation of turbulent channel flow with spanwise rotation, J. Fluid Mech. **788**, 42 (2016).
[43] Y. J. Dai, W. X. Huang, and C. X. Xu, Effects of Taylor-Görtler vortices on turbulent flows in a spanwise-rotating channel, Phys. Fluids **28**, 115104 (2016).
[44] G. Brethouwer, Linear instabilities and recurring bursts of turbulence in rotating channel flow simulations, Phys. Rev. Fluids **1**, 054404 (2016).
[45] A. Hsieh and S. Biringen, The minimal flow unit in complex turbulent flows, Phys. Fluids **28**, 125102 (2016).
[46] G. Brethouwer, Statistics and structure of spanwise rotating turbulent channel flow at moderate Reynolds numbers, J. Fluid Mech. **828**, 424 (2017).
[47] R. Benzi, S. Ciliberto, R. Tripiccione, C. Baudet, F. Massaioli, and S. Succi, Extended self-similarity in turbulent flows, Phys. Rev. E **48**, R29 (1993).
[48] R. Benzi, S. Ciliberto, C. Baudet, and G. R. Chavarria, On the scaling of three-dimensional homogeneous and isotropic turbulence, Physica D **80**, 385 (1995).
[49] R. Benzi, L. Biferale, S. Ciliberto, M. V. Struglia, and R. Tripiccione, Generalized scaling in fully developed turbulence, Physica D **96**, 162 (1996).
[50] R. Benzi, M. V. Struglia, and R. Tripiccione, Extended self-similarity in numerical simulations of three-dimensional anisotropic turbulence, Phys. Rev. E **53**, R5565 (1996).

[51] R. Benzi, L. Biferale, S. Ciliberto, M. V. Struglia, and R. Tripiccione, On the intermittent energy transfer at viscous scales in turbulent flows, Europhys. Lett. **32**, 709 (1995).

[52] S. Grossmann, D. Lohse, and A. Reeh, Application of extended self-similarity in turbulence, Phys. Rev. E **56**, 5473 (1997).

[53] C. Meneveau, Transition between viscous and inertial-range scaling of turbulence structure functions, Phys. Rev. E **54**, 3657 (1996).